

## Review

# Light on osteoarthritic joint: from bench to bed

Yingying Zhou<sup>1,2\*</sup>, Junguo Ni<sup>1\*</sup>, Chunyi Wen<sup>1,2,3✉</sup>, Puxiang Lai<sup>1,2,4✉</sup>

1. Department of Biomedical Engineering, The Hong Kong Polytechnic University, Hong Kong SAR
2. The Hong Kong Polytechnic University Shenzhen Research Institute, Shenzhen, China
3. Research Institute of Smart Ageing, The Hong Kong Polytechnic University, HKSAR
4. Photonics Research Institute, The Hong Kong Polytechnic University, HKSAR

\* These authors contributed equally

✉ Corresponding authors: Chunyi Wen: [chunyi.wen@polyu.edu.hk](mailto:chunyi.wen@polyu.edu.hk). Puxiang Lai: [puxiang.lai@polyu.edu.hk](mailto:puxiang.lai@polyu.edu.hk).© The author(s). This is an open access article distributed under the terms of the Creative Commons Attribution License (<https://creativecommons.org/licenses/by/4.0/>). See <http://ivyspring.com/terms> for full terms and conditions.

Received: 2021.06.28; Accepted: 2021.11.08; Published: 2022.01.01

## Abstract

Osteoarthritis (OA) is one of the rapidly growing disability-associated conditions with population aging worldwide. There is a pressing need for precise diagnosis and timely intervention for OA in the early stage. Current clinical imaging modalities, including pain radiography, magnetic resonance imaging, ultrasound, and optical coherent tomography, are limited to provide structural changes when the damage has been established or advanced. It prompts further endeavors in search of novel functional and molecular imaging, which potentially enables early diagnosis and intervention of OA. A hybrid imaging modality based on photothermal effects, photoacoustic imaging, has drawn wide attention in recent years and has seen a variety of biomedical applications, due to its great performance in yielding high-contrast and high-resolution images from structure to function, from tissue down to molecular levels, from animals to human subjects. Photoacoustic imaging has witnessed gratifying potentials and preliminary effects in OA diagnosis. Regarding the treatment of OA, photothermal-triggered therapy has exhibited its attractions for enhanced therapeutic outcomes. In this narrative review, we will discuss photoacoustic imaging for the diagnosis and monitoring of OA at different stages. Structural, functional, and molecular parameter changes associated with OA joints captured by photoacoustics will be summarized, forming the diagnosis perspective of the review. Photothermal therapy applications related to OA will also be discussed herein. Lastly, relevant clinical applications and its potential solutions to extend photoacoustic imaging to deeper OA situations have been proposed. Although some aspects may not be covered, this mini review provides a better understanding of the diagnosis and treatment of OA with exciting innovations based on tissue photothermal effects. It may also inspire more explorations in the field towards earlier and better theranostics of OA.

Key words: Osteoarthritis; photoacoustic imaging; photothermal therapy; cartilage; synovium

## Introduction

Being one of the rapidly growing disability-associated conditions worldwide, Osteoarthritis (OA) is a leading cause of chronic pain and poor quality of life especially for older adults [1]. Currently, there is no effective cure for OA when articular cartilage damage is established [2], which prompts an urgent need for early detection and intervention of the disease prior to irreversible joint damage.

The key problem in early detection and intervention of OA is a historical observation on the disparity of structural damage and symptomatic

severity [3]. Current imaging modalities, radiography (X-ray), positron emission tomography (PET), magnetic resonance imaging (MRI), optical coherence tomography (OCT), and ultrasound (US) [4, 5], are limited to provide structural information and fail to elucidate functional deficit and pain severity. The capacities of these imaging modalities are summarized in Table 1. Among them, X-ray is a classic method to assess bony changes, especially joint space width (JSW) and osteophytes, but it is radiative and has limitations in imaging soft tissue and

subchondral structures [6], typical symptoms of early OA. For MRI, US, and OCT, they are nonradioactive and provide more detailed imaging information that is impossible with X-ray, enhancing the diagnosis of OA. However, MRI is costly and its accessibility is limited, having a long waiting list for public hospital patients even in some developed regions like Hong Kong. Moreover, the imaging modality is contraindicated for patients wearing implanted devices [6]. For US imaging, it has low contrast, strong boundary effects, and insufficient sensitivity to early OA changes, being lack of standardized definitions [6]. OCT, in comparison, achieves a better balance among cost, sensitivity, and contrast, but suffers a shallow imaging depth due to strong scattering of light in tissue, making it difficult for noninvasive diagnosis of OA at depths. Although the PET can obtain active metabolism in articular and periarticular tissues, thus allowing evolution of metabolic changes within the bone. This method lacks the needed spatial resolution for studying the microenvironment and relies on radioactively labeled exogenous tracers.

**Table 1.** Summary of current imaging modalities' capacities for OA diagnosis

Imaging modality	Capacities
X-ray	Evaluation of osteophyte formation, joint space narrowing (JNS), and subchondral sclerosis or subchondral cysts. [4-6]
PET	Provide metabolism information in articular and periarticular tissues. [5]
MRI	Offer superb soft tissue contrast, which is used in assessment of cartilage lesions. [4-6]
OCT	Generate cross-sectional images of articular cartilage and provide quantitative information about the disease state of articular cartilage; sensitive to collagen structural changes. [4-6]
US	Identification of tibiofemoral osteophytes, medial meniscal extrusion, and medial femoral cartilage morphological degeneration [4-6]

The aforementioned imaging modalities including X-ray and MRI have achieved excellent penetration for anatomical imaging from macro-scale aspect. In addition, the PET and single-photon emission computed tomography (SPECT) are highly sensitive to the radiolabelled molecular probes, which realizes deep penetration. The optical microscopes can describe biological phenomena with subcellular and subcellular resolution in detail at superficial depths from micro-scale side. However, different imaging contrast mechanisms and length scales of these imaging tools hinder the multi-scale study of biological problems. Therefore, a continuum from micro to macro imaging is desired to be established in life science. Photoacoustic (PA) imaging is a hybrid imaging modality based on photothermal effects.

Through converting diffused light into non- or weak-scattered ultrasonic waves, PA imaging combines the advantages of optical contrast and ultrasound detection [7-10]. It can yield high-contrast and high-resolution images of different subsurface tissues to probe molecular events or changes, and it has been proven to be capable of multiscale imaging from micro to macro fields in life science, sharing a consistent contrast mechanism [11]. Depending on how photoacoustic signals are received and reconstructed to form the image, photoacoustic imaging can roughly be divided into two categories, photoacoustic microscopy (PAM) and photoacoustic computed tomography (PACT). As illustrated in Figure 1(A), usually PAM has a higher resolution but a shallower penetration depth compared with PACT due to trade-off between the optical spatial resolution and penetration depth. Combining PAM and PACT, photoacoustic imaging can achieve a multiscale ability, as shown in Figures 1(B-D). More importantly, many endogenous tissue constituents, such as oxyhemoglobin, deoxyhemoglobin, and water, possess distinctive optical absorption spectra and hence can be used as natural contrasts to be captured under optical illumination of different wavelengths to indicate status of targets, providing label-free functional and molecular specific information [12]. In scenarios where the endogenous contrasts cannot yield sufficient signal-to-noise ratio (SNR), for example to detect cancer from blood rich organs like liver, exogenous contrast agents can be added and accumulate at the region of interest, which leads to increased contrast and highlighted object imaging [13-16].

Benefiting from its attractive advantages, photoacoustic imaging has been widely used in early diagnosis and treatment monitoring of a variety of diseases, such as cancers [18, 20-22], vascular diseases [23, 24], and brain conditions [25, 26]. Lin *et al.* developed a single-breath-hold PACT system and successfully revealed a higher blood vessel density associated with tumors in human breasts with high resolution in deep penetration depth [18]. Jo *et al.* reported an *in vivo* quantitative tumor pH mapping nanotechnology with nanoprobe by multi-wavelength PA imaging, which holds great potential for both research on and clinical management of a variety of cancers [27]. Liu *et al.* successfully delineated *in vivo* brain gliomas with the help of exogenous contrast through near-infrared PA imaging [26]. Long before the structural and functional parameters including vascular morphology, blood oxygenation, blood flow and oxygen metabolism have been realized by PA imaging [19]. Recently, there also has a growing body of interests in

application of PA imaging for OA research in both animals and humans. Hereby, we discussed current development of PA imaging at the crossroad of optics, and biomaterials and biomedicine, and how the PA imaging applied in the early stage of OA for diagnostic purpose.

Precise diagnosis of early-stage OA also benefits timely treatment of the disease. Current state-of-the-art photothermal technology has emerged as a novel OA therapy [28, 29]. The mechanism of photothermal therapy (PTT) in some way is akin to PA, i.e., converting light to heat due to tissue absorption. Thus, PTT can achieve non-invasive treatment, which has already been verified in many studies [30-32].

In this narrative review, we aim to discuss the mechanism and feasibility of noninvasive photoacoustic diagnosis of OA in its early stage and monitoring the disease progression, including both structural and microenvironment alterations. The application of photothermal-triggered drug release for OA is also discussed herein. Lastly, relevant clinical applications are discussed. It is hoped that the review, although some aspects may not be covered due to the limit of manuscript space, can deepen the understanding of diagnosis and treatment of OA with photothermal effects and inspire more explorations in the field towards more clinical trials.

## Evolution of osteoarthritis

OA is one of the most common chronic arthritic diseases, and it is also the main cause of disability and joint dysfunction in the elderly nowadays [33]. The pathophysiology of OA is very complicated. It is related to age, gender, obesity, diet, genetic factors,

and many other factors at the individual level [34-36]. The typical characterization of OA is the degeneration of articular cartilage and elevated chondrocyte mortality [37]. Possible reasons include mechanical and biological factors that lead to degradation and synthesis imbalance of chondrocytes, extracellular matrix, and subchondral bone [38, 39]. These structural and functional variations are inherently accompanied with optical properties changes at single or multiple wavelengths, which can potentially be sensed or mapped by PA imaging. Therefore, this section discusses the evolution of joint OA from structure damages and microenvironment changes, respectively (Figure 2), forming the physiological basis of PA diagnosis of OA joints.

## Structure damages of joint tissue in OA

Our human body is composed of many joints, whose structures are usually complex and distinct from one another. Among these joints, many, such as knee, finger, hip, and spine, could develop OA symptoms [40-42]. These symptoms, according to extensive etiological and pathological studies in the field, often involve structure change or damages in the joints, which gradually evolves and emerges as the whole joint disease [39, 43]. For instance, knee joints are mainly organized by articular cartilage, bones (femur, tibia and fibula), synovium, tendons, ligaments, and meniscus [44]. Abnormalities of these constituents are often associated with OA progression [43]. Hence, one of the key characteristics of OA diagnosis is whether these structural changes can be imaged or sensed, for which PA could play a promising role.

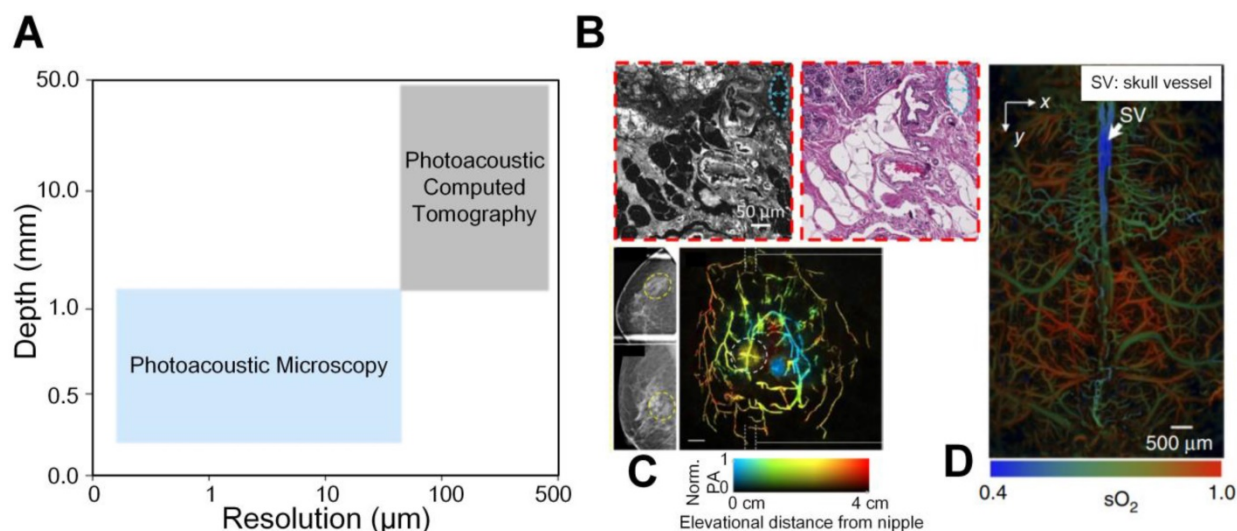


**Figure 1.** (A) A continuum from micro to macro by photoacoustic imaging. (B) An example of micro-scale structural photoacoustic imaging. Photoacoustic microscopy and hematoxylin and eosin-stained figures of normal human breast tissue [17]. (C) An example of macro-scale structural photoacoustic imaging. Photoacoustic computed tomography of human breast cancer [18]. (D) An example of micro-scale functional photoacoustic imaging. Oxygen saturation of mouse brain [19]. Adapted with permission from [17-19]. Copyright © 2017, Copyright © 2018, and Copyright © 2015 Springer Nature.

Especially, articular cartilage is a critical pivotal part of joints; its damage is observed in nearly all OA patients, and hence its degeneration is often referred to as one of the hallmarks of OA [45]. Macroscopically, articular cartilage changes associated with OA include, but are not limited to, cartilage softening, fibrillation, and erosion [46]. Although the morphology changes are not significant at the early stage of OA, histologically, the superficial zone of articular cartilage appears to change first, which can be visually observed [47]. This damage will become more serious as the OA condition worsens, from surface contour lightly unregulated until the whole cartilage structure completely destroyed [48]. Likewise, observing the morphology of subchondral bone altered is another essential index in OA diagnosis. In past decades, large efforts have been made to demonstrate the importance of abnormal subchondral bone remodeling in OA development [49, 50]. It has been reported that subchondral bone integrity will be influenced with the OA development and subchondral bone plate thinner, and more porous could be detected in early OA [51]. Moreover, studies no matter in animal models or in specimens from OA patients emphasize sclerosis of subchondral bone, joint space narrowing, and osteophyte formation in late stages of OA [52-54]. Concomitantly, swelling of synovium and the injury of other components (i.e., meniscus, ligaments, etc.) of joint are also the major sites of macroscopic changes in the OA process [43, 55, 56]. As such, PA could be used to diagnose and evaluate the severity of OA by imaging the structure of joints and its changes.

### **Functional (microenvironmental) changes in OA joints**

That said, OA is a slow progression disease; the deformation of anatomical structures in the joints is slight and might be hard to be detected at the initial stage [57]. In comparison, microenvironmental communications happened throughout the entire OA progression, presenting parameter variations before the morphology injuries [58]. These microenvironment changes could lead to alterations of tissue optical properties, such as absorption and/or scattering spectrum, which provides potentials for early diagnosis of OA joints with photoacoustic methods.

Abundant extracellular matrix and chondrocytes embedded within it compose articular cartilage [59]. For natural and healthy cartilage, water, collagen II, and proteoglycan are the primary compositions [46]. At the initial stage of OA, the form of proteoglycans begins to change, causing shorter chain length and lower percentage of normal macromolecular

complexes [46]. Meanwhile, the water content increases in the cartilage matrix, which softens the articular cartilage and changes the biomechanical feature [60]. These changes further induce chondrocyte abnormal activities, oversecrete proteolytic enzymes and inflammatory cytokines, and finally disrupt the collagen network, such as matrix metalloproteinases (MMPs), nitric oxide (NO), reactive oxygen species (ROS), tumor necrosis factor- $\alpha$  (TNF- $\alpha$ ), interleukin-1 $\beta$  (IL-1 $\beta$ ), etc [37, 61-63].

In the subchondral bone, the disorder of bone metabolism is the direct consequence of abnormal cell-to-cell communications [64]. It is well known that the amount of blood vessels increases in subchondral bone and vessel erosion into the avascular cartilage with OA progression [65, 66], as illustrated in Figure 2. A rabbit's study demonstrates that angiogenic activity of subchondral bone achieves the highest level in the early to the progressive stage OA, and then decreases back to the normal level in the late stage of OA [67]. Subsequently, more recent research finds that subchondral bone angiogenesis is induced by abnormal rise of platelet-derived growth factor-BB [68]. Moreover, accumulating evidence has shown that hypervascularization and subchondral bone edema occur earlier than cartilage lesions [69-72], influencing the microenvironment like water content, hemoglobin concentration, and blood oxygenation, which could be used as the early diagnostic indicator of OA.

*Taken together*, the structure alterations due to OA are mainly reflected by volume loss of articular cartilage, thickening of subchondral bone, and the formation of osteophyte, whose PA imaging features could be used as the criteria for the diagnosis of OA. However, these visual changes of joints usually do not emerge until the late stage of OA, which limits the treatment choice of patients. Detecting initial OA-like variations in joints as early as possible is highly desired yet still challenging in clinical diagnosis. Fortunately, in addition to structure imaging, PA is also capable to track the changes of microenvironment with disease progression based on the expression level of molecules [73-75], which strongly supports the hypothesis of PA for early diagnosis of OA as well as dynamic monitoring of OA progression.

### **Photoacoustic diagnosis of osteoarthritis**

#### **Structure changes in OA observed with PA**

As different tissue constituents as well as their alignment and distribution result in their characteristic absorption spectra, PA imaging can be applied to observe the structural changes associated

with OA based on their wavelength-dependent property [76].

### Sponge bone

Izumi *et al.* designed an ultrasonic and photoacoustic dual-mode imaging platform to investigate the divergences between normal rat knee joints and OA joints [77, 78]. In their findings, compared with normal joints, the sponge layer expresses considerably stronger PA signals in the OA joints, while the US reflections are almost identical in two scenarios. The trend can be seen more clearly from the quantitative averaged US and PA intensities in the sponge layer between the healthy joints and OA joints: the PA signal amplitudes induce obvious differences between normal and OA joints, while the US values show much fewer variations. The enhanced contrast in PA is probably associated with the increased optical absorption from more blood due to vascularization and inflammation as illustrated in Figure 2. It also suggests that PA potentially provides a better indicator than US does to visualize the sponge bone of OA from normal joints.

### Cartilage and subchondral bone

In addition to the elevation of PA signals in the sponge bone of OA joints compared to normal joints, Hagiwara *et al.* investigated the PA/US signals changes in the subchondral bone and cartilages by sequential monitoring of immobilized knees in rats [79]. The white dashed arrow in Figure 3(A) points to the subchondral bone and the upper part of it is cartilage. The US mode in the PA system demonstrates that the surface of the articular cartilage becomes irregular with a longer duration of immobilization, while the PA mode shows a dramatic signal increase in the subchondral bone with long immobilization. Quantified PA changes are shown in Figures 3(B-C). As seen, the PA signals show limited differences in cartilages before and after immobilization. In contrast, significant variations are observed in the subchondral bone, which indicates that the PA signal intensities elevates in the subchondral bone with the time of immobilization to the keen joints. Therefore, the combined US/PA information can be utilized to assess the OA joints from the cartilage and subchondral bone changes.

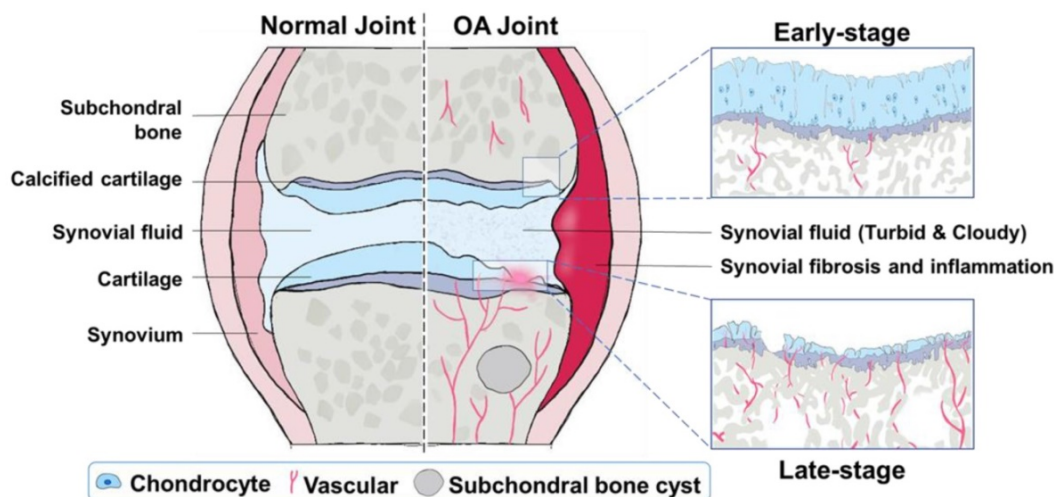


**Figure 2.** Illustration of structural and microenvironment transformations during OA progression. Compared with normal joints, OA joints will undergo different degrees of changes with the OA progression. In early-stage OA, the surface contour of cartilage is lightly unregulated, the superficial zone of articular cartilage splits slightly, the subchondral bone plate is thinner yet more porous, and a few vessels erode into the avascular cartilage. In late-stage OA, the whole cartilage structure is completely destroyed, which is usually accompanied with subchondral bone sclerosis, joint space narrowing, osteophyte formation, and more vessels erosion into the cartilage.

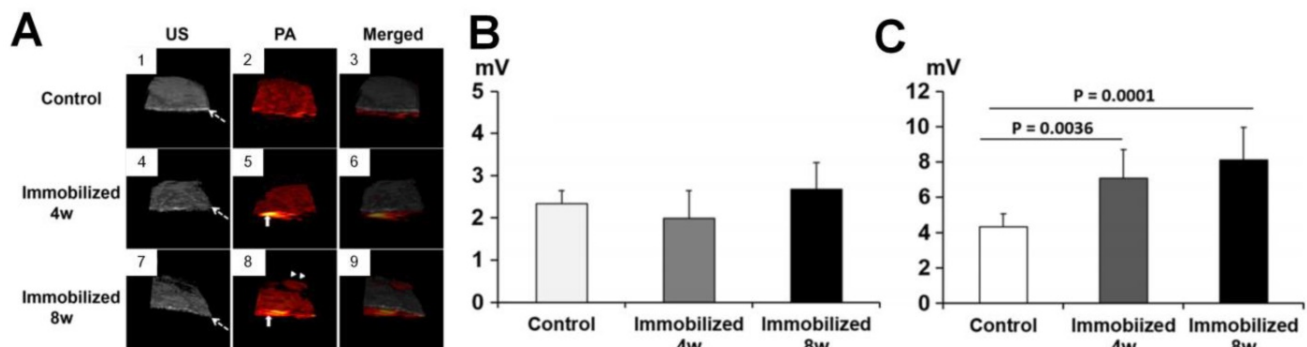


**Figure 3.** (A) US, PA and the merged images of knee joints in different stages. (B-C) Quantified PA amplitudes at different stages from cartilage and subchondral bone, respectively. Figures adapted with permission from Ref [79]. Copyright © 2015, Elsevier.

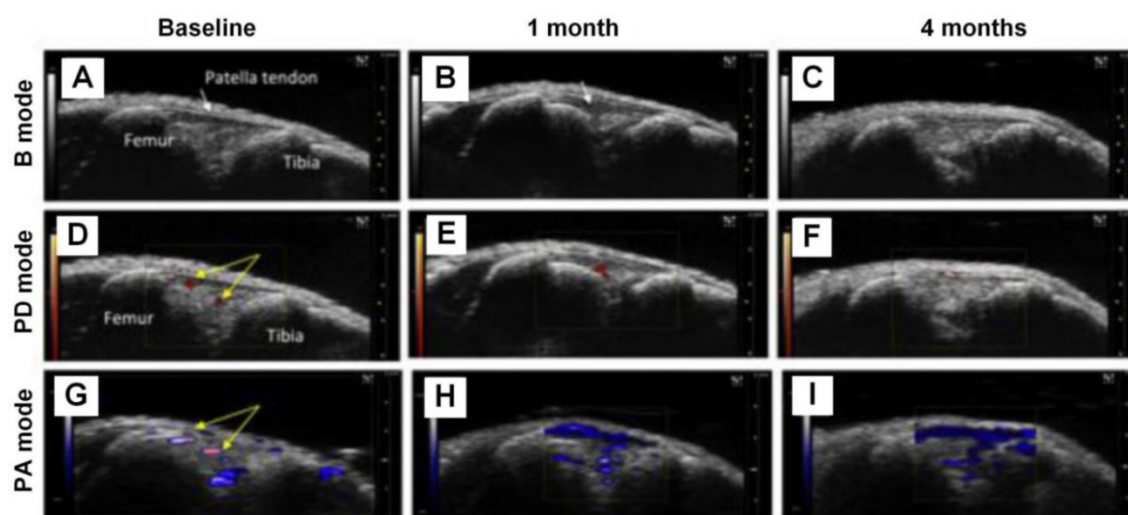


**Figure 4.** DMM knee joints at different stages being visualized with B mode ultrasound, PD mode ultrasound, and PA imaging, respectively. (A)-(C), B mode ultrasound images of the knee joints at baseline, 1 month, and 4 months, respectively. (D)-(F), PD mode ultrasound images of the knee joints at baseline, 1 month, and 4 months, respectively. (G)-(I), PA images of the knee joints at baseline, 1 month, and 4 months, respectively. Figures adapted with permission from Ref [80]. Copyright © 2018, Elsevier.

### Functional (microenvironmental) changes in OA obtained with PA

The early diagnosis of OA can help patients relieve pain timely and improve therapy outcomes. However, early-stage OA may exhibit few or very light changes in structures, which may not be easily sensed or detected by PA. Under this circumstance, capturing the changes of microenvironmental parameters, such as metabolism, blood information, and optical absorption, in OA joints possesses critical significance.

#### Vascularity and hypoxic status

Inflammation of the synovium is another symptom of OA. Liu *et al.* proposed to use PA imaging, combined with B mode ultrasound and Power Doppler (PD) ultrasound, to monitor the synovial tissue vascularity and hypoxic status changes in the knee joints [80]. The results are shown in Figure 4, from which one can see that in 1 month and 4 months post destabilization of medial meniscus (DMM) surgery, PA signals increase significantly. Moreover, based on PA signals obtained at two optical wavelengths (750 nm and 850 nm in this experiment), the hemoglobin oxygen saturation information can be extracted, which suggests a dramatic decrease in the DMM knee joints from normal joints, and the degree of declination is closely related with the severity of OA (lower oxygen saturation in severer OA joints). These results are well verified in the B mode and PD mode images, demonstrating the feasibility of utilizing PA imaging to monitor the variations of vasculature and oxygen saturation in the OA joints correctly.

### Hemoglobin concentration, water contents, and acoustic velocities

With multi-wavelength PA imaging, Xiao *et al.* quantitatively compared several functional parameters, including oxyhemoglobin ( $\text{HbO}_2$ ), deoxyhemoglobin (Hb), water contents, and acoustic velocities between normal distal interphalangeal (DIP) and OA joints [81]. The extracted parameter images are listed in Figures 5(A-H). As shown, significantly increased water contents, declined oxygen saturation, and elevated acoustic velocity are observed in OA joints as a comparison with normal joints. Later, the same group further modified their system into a 3D multispectral quantitative version and reported the difference of hemoglobin concentration and oxygen saturation in osteoarthritic phalanges and soft joint tissues in joint cavities between the OA and healthy groups [82]. An elevated hemoglobin concentrations and declined oxygen saturations in these two different joint tissues were observed, which is consistent with their previous findings [81, 83].

#### $\text{H}_2\text{O}_2$ expression

Apart from the vascular parameters and oxygen saturation changes in the synovial tissue for OA joints, there is typical excessive production of oxidative species, such as  $\text{H}_2\text{O}_2$ , at the inflammation sites in the synovium. Based on that mechanism, Li *et al.* proposed a dual ratiometric surface-enhanced Raman scattering (SERS) and PA imaging to monitor and quantify the level of  $\text{H}_2\text{O}_2$  in the knee OA of rabbits with core-satellite nanoprobe [84]. As shown in Figure 6, the  $\text{H}_2\text{O}_2$  concentration is much higher in the OA knee, but the I2228/I1418 (the SERS intensity

at 2228 nm divided by the SERS intensity at 1418 nm) undergoes significant decline with time after nanoparticles injection into the OA knee while the ratio keeps fairly stable in the normal (control) knee. For PA signals in the OA knee, it experiences fuzzy changes with time at both 750 and 1250 nm, but the signal ratio ( $PA_{\Delta 750}/PA_{\Delta 1250}$ ) between these two wavelengths does show an obvious growth after injection, which also suggests increased  $H_2O_2$  level. The study also suggests the combination of SERS and

PA imaging as well as their signal ratios help to precisely locate the OA position. Later on, a similar study was realized by the same group with only PA imaging enhanced by nanoparticles [85]. In this study, the  $H_2O_2$  expression at different stages of OA is quantified based on the ratios of PA signals at two wavelengths. The results suggest that in the OA joints, the signal ratio is significantly different from the normal joints due to higher expression of  $H_2O_2$  and the absorption shifting of nanoparticles.

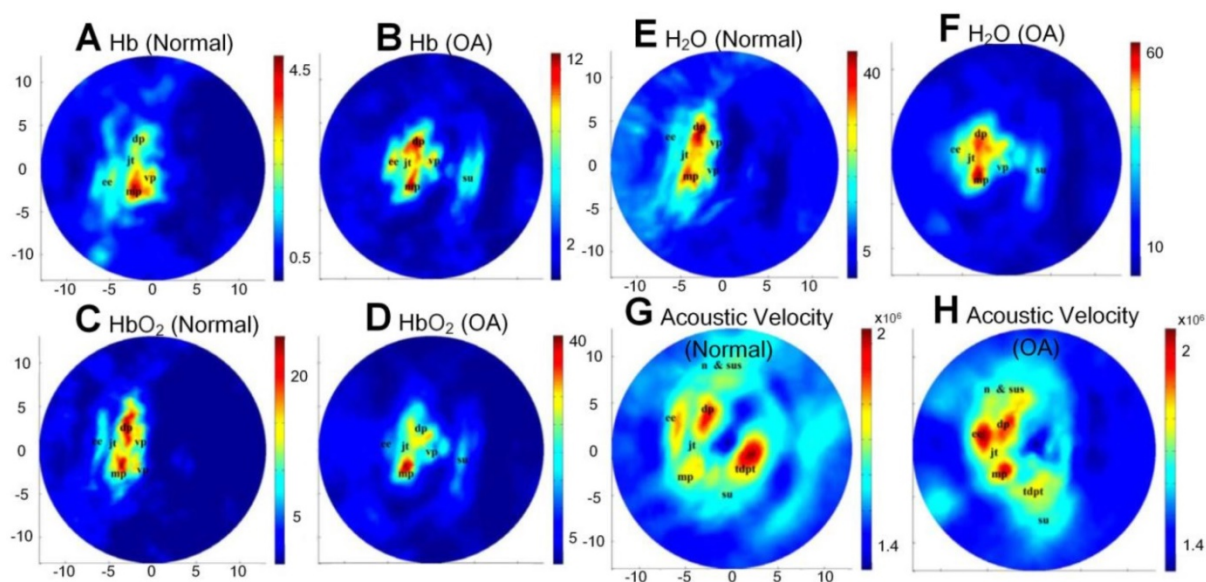


**Figure 5.** (A)-(H) Different functional parameters (Hb, HbO<sub>2</sub>, water contents, and acoustic velocity) of normal and OA joints, respectively, through multi-wavelength PA imaging. Figures adapted with permission from Ref. [81]. Copyright © 2010, The Optical Society.

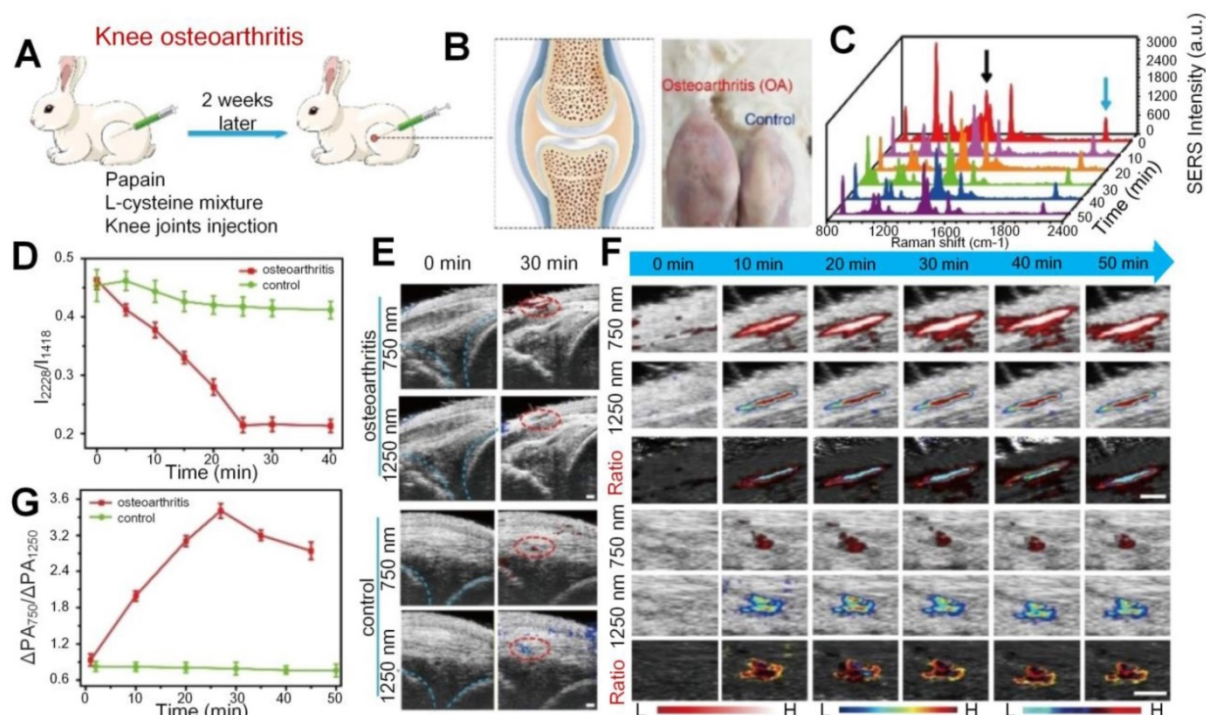


**Figure 6.** (A) *In vivo* knee OA model establishment process. (B) The cartoon figure (left) of knee OA and the photos (right) of OA and normal knees. (C) SERS spectra. (D)  $I_{2228}/I_{1418}$  SERS intensity change versus time. (E) Ultrasound (US)/PA images of the OA and normal knees. PA signals are marked in red circles. (F) 750 nm, 1250 nm, and the ratiometric PA images. (G) Ratiometric  $PA_{750}/PA_{1250}$  value versus time for OA and normal knees. Scale bar is 1 mm in (F). Figures adapted with permission from Ref. [84]. Copyright © 2020, Wiley-VCH GmbH.

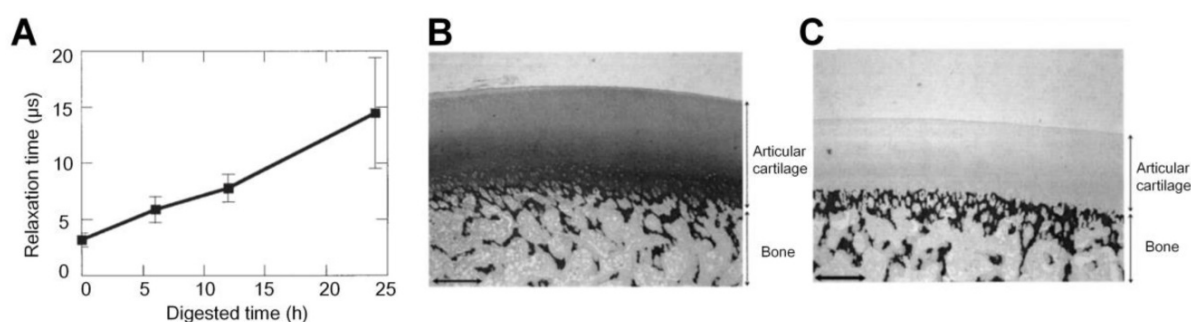


**Figure 7.** (A) Relaxation time of PA signals at different degrees of cartilage damage. (B)-(C) Histological results of normal porcine cartilage and 12 hours trypsin treated cartilage, respectively. Figures adapted with permission Ref.[86]. Copyright © 2006, Wiley-Liss, Inc.

### Viscoelastic property

In addition to the aforementioned functional parameters, PA can also be applied to assess the viscoelastic properties of cartilage damaged at different degrees. Ishihara *et al.* developed a PA viscoelastic tissue measurement method to diagnose cartilages in the OA joints [86] and to evaluate the viscoelastic property of the tissue-engineered cartilages [87-90]. As shown in Figure 7, the relaxation time of PA signals, which can be used to compute the viscoelastic characteristics of tissue, is approximately a linear function of the digested time of trypsin treatment. The trypsin was used here to simulate the damage degree of cartilages, which was confirmed with the histological results shown in Figures 7(B-C). These results demonstrate the PA viscoelastic measurement method can be used to delineate the degree of cartilage damage in OA. Ukai *et al.* also found that the laser-induced PA (LIPA) measured viscoelastic results had an approximately (positive) linear relationship with the cartilage damage grade, which is well consistent with the MRI results discussed in the same study [91].

### Probe-enhanced PA imaging of OA

While endogenous tissue constituents, such as cartilage, subchondral bone, water, and hemoglobin, provide inherent potentials for structure or function-based diagnosis of OA joints with PA imaging, extraneous agents, such as nanoparticles, can be applied to achieve enhanced detection contrast, sensitivity, and specificity of OA symptoms. Current photoacoustic nanoparticles applied in OA can be divided into two categories, inorganic and organic. Most of them are multiple modified for specific applications. Inorganic photoacoustic nanoprobe, such as Ag shell coated Pd-tipped gold nanorods (Au-Pd@Ag NR) developed by Ye *et al.* can quantitatively evaluate the inflammation status by  $H_2O_2$  levels and precisely treat it with Ag ions release in the OA sites [85]. Another probe, core-satellite gold nanostructure, was reported by the same group also

can precisely detect the  $H_2O_2$  levels in the inflammation positions [84]. The reported organic nanoparticles include articular cartilage-target poly-L-lysine-encapsulated melanin nanoparticles (PLLMNPs) [92, 93] and inflammatory-bonded PEGylated, phenylboronic acid modified L-DOPA pro-antioxidant (pPAD) [94]. Both of them serve as a good photoacoustic contrast to reveal the OA status from different aspects. Take cartilage degeneration as an example; the anionic glycosaminoglycan (GAGs) contents will decline with the severe degree of OA. In 2018, Chen *et al.* [92] designed cationic poly-L-lysine-encapsulated melanin nanoparticles (PLL-MNPs) to function as photoacoustic contrast agent that can target the GAGs contents of articular degeneration in OA due to the strong electrostatic interaction between the PLL-MNPs and GAGs. The principle of the probe design is shown in Figure 8(A). The PA signals of PLL-MNPs targeted with GAGs are much higher than normal melanin nanoparticles (MNP) and other control groups, such as PBS injection and blocking at wavelength of 680 nm, as illustrated in Figure 8(B). The *in vivo* qualitative and quantitative results in Figures 8 (C1 and C4) further show that PLL-MNPs in normal joints with high contents of GAGs exhibit PA signals that are about two folds stronger than the signals from the OA joint possessing lower GAGs contents. As shown in Figures 8 (C2 and C5), researchers have also applied this PLL-MNPs for monitoring the treatment outcomes after 4 weeks hyaluronic acid (HA, one kind of drug to improve cartilage degeneration) injection. Note that the nanoparticle-enhanced PA signals become considerably stronger after the treatment for early-stage OA, but for late-stage OA the PA signals experience much fewer variations, indicating better therapeutic efficacy to early-stage OA than to late-stage OA. This result is consistent with the Mankin score study that uses safranin-O to stain GAGs; in this study, a lower Mankin score represents an improved condition. Based on this probe, the same group further tested the ability of PLL-MNPs

enhanced PA to differentiate different GAGs concentrations in cartilage explants. It is confirmed that molecularly enhanced PA signals are capable of reflecting the course of OA *in vivo*, which has great significance in the monitoring of clinical therapy [93].

## Photothermal-triggered drug release therapy of OA

Thus far, we have discussed the feasibility of utilizing PA methods to diagnose and monitor the therapeutic outcome of OA. It is hence necessary to introduce photothermal therapy, a treatment method based on photothermal effects and has gained great attention to treat abnormal tissues like tumors [28]. The mechanism of PTT in some way is akin to PA, *i.e.*, through converting light to heat due to tissue absorption. That said, PTT typically uses near-infrared light to treat the target with enhanced heat and penetration in tissue, and it must be assured that the surrounding cells and tissues are minimally affected by light illumination. Thus, the usage of exogenous PA contrast agents is usually desired to ensure that the target, accumulated (actively or passively) with molecular probes, has an absorption spectrum that is distinct from that of normal tissues. With light illumination at the absorption peak wavelength of the probe, at the target position, the PTT efficiency can be greatly increased and the treatment outcomes can be ensured, while tissue damage to the surroundings can be suppressed. In current OA treatment, photothermal effect was served as an efficient tool through converting light to heat with the help of multifunctional nanoparticles, which is then activated by the heat to release the therapeutic drugs in OA joints. The multifunctional nanoprobes

can transfer the light to heat with high efficiency and carry the therapeutic drug simultaneously. For example, Chen *et al.* synthesized photothermal-triggered NO nanogenerators, NO-Hb@siRNA@PLGA-PEG (NHsPP) nanoparticles, which enabled precise NO, siRNA, and PTT treatment on the inflamed OA simultaneously. The joint treatment significantly enhanced the therapeutic efficiency by suppressing macrophage inflammation in comparison to any individual method alone under 650 nm laser irradiation [29]. The reaction process is illustrated in Figure 9 (A), where two signal pathways including up-regulation of AMPK and down-regulation of Notch-1 were triggered under the 650 nm laser irradiation after injection of the NHsPP nanoparticles. Both pathways can promote the macrophage inflammatory response and thus accelerate the anti-inflammatory outcomes. As shown in Figures 9(B-C), in contrast to normal joints, the NHsPP nanoparticles could precisely accumulate at the inflamed sites due to the specific combination of Notch 1-si RNA within a short time and remained in the region for nearly 24 hours. The PTT high efficiency was also confirmed in the OA joints under laser irradiation, as indicated in (D) and (E). Different parameters in OA joints, including mean clinical scores, inflammatory cytokines (TNF- $\alpha$ , IL-1 $\beta$  and IL-6), Mac-3 (a macrophage marker), and cartilage erosion degrees, were compared among different treatment groups, and the results are shown in Figures 9(F-K). All these parameters demonstrate that the NHsPP nanoparticle-assisted photothermic guided effect yield promising therapeutic efficiency and the recovery outcomes are near to the normal groups.

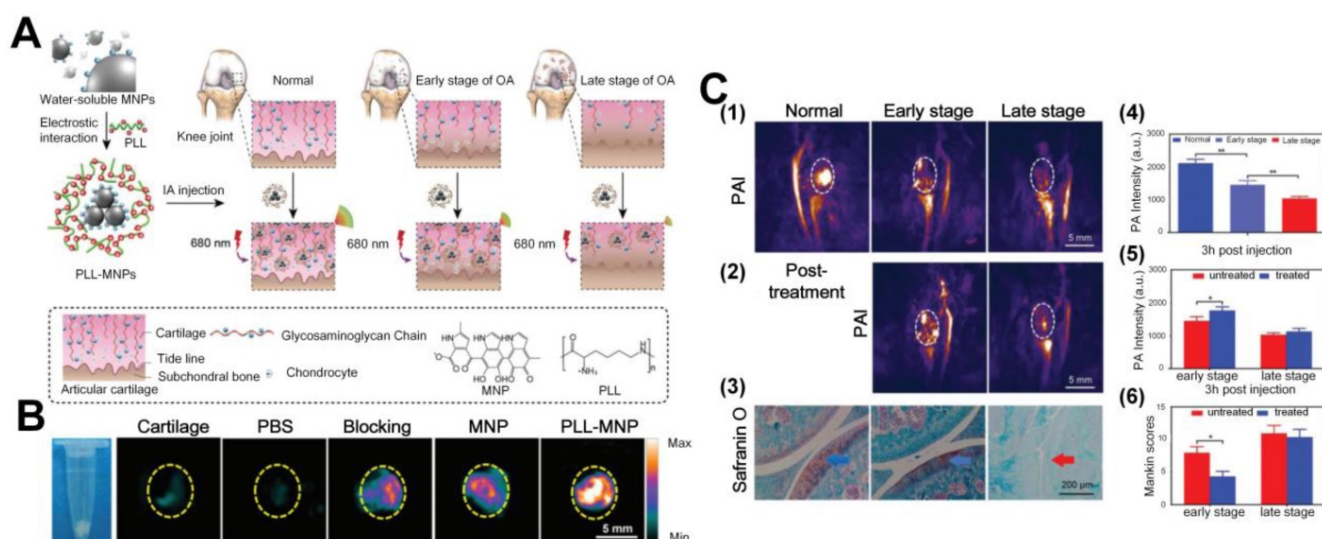


**Figure 8.** (A) Schematic diagram of the preparation of PLL-MNPs and the mechanism of diagnosis of OA cartilage degeneration with PAI. (B) PA images of cartilage after immersion in different contrast media for 24 hours. Scale bar: 5 mm. (C) PA images of early and late stages of OA with PLL-MNPs, PA post-treatment monitoring after hyaluronic acid (HA) injection, and its comparison with Mankin scoring system results. Figures adapted with permission from Ref. [92]. Copyright © 2018, Royal Society of Chemistry.

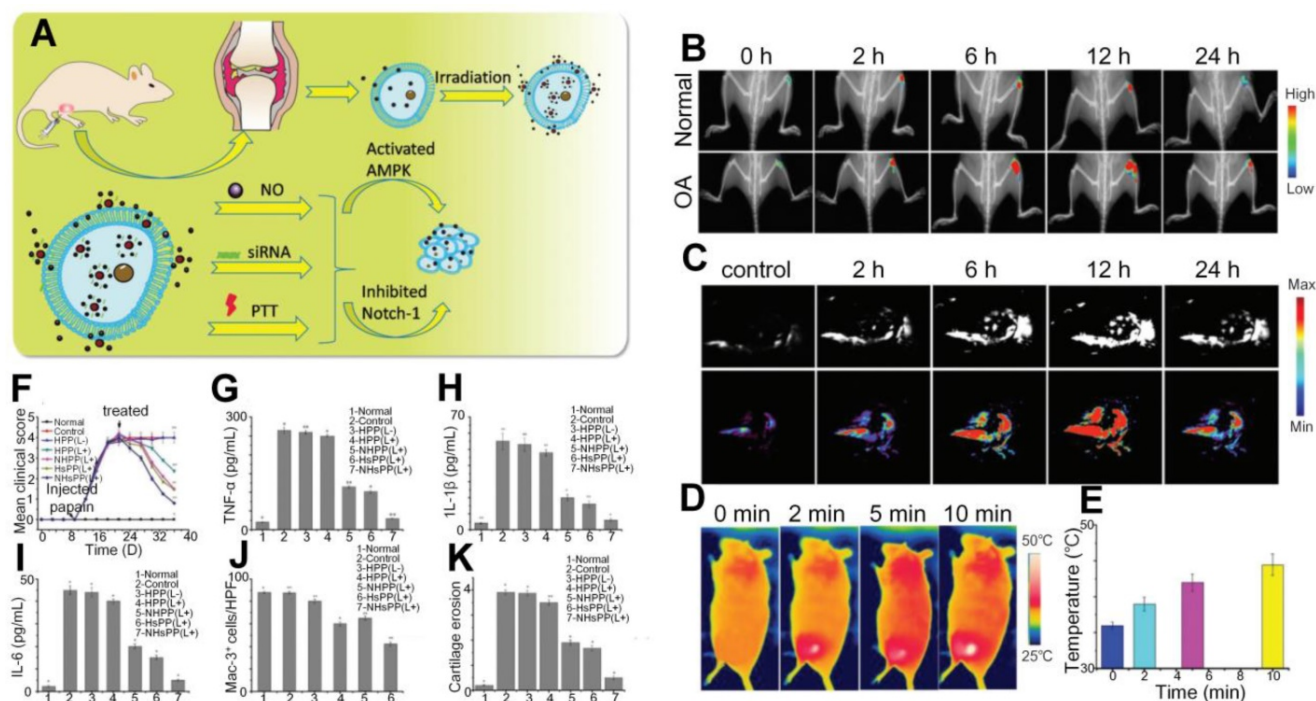


**Figure 9.** (A) Reaction process of the NHsPP nanoparticles in the OA after light illumination. (B) Spatial distributions of NHsPP nanoparticles in the OA and normal joints at different times. (C) PA signals of the nanoparticles in the OA joints at different time. (D) Nanoparticle-enhanced photothermal images under laser irradiation. (E) The temperatures changes with time under the photothermal effect. (F-K) Semi-quantitative comparisons between different treatment methods as a function of time. Figures adapted with permission from Ref. [29]. Copyright © 2019, Royal Society of Chemistry.

Zhao *et al.* designed another nanoprobe, MoS<sub>2</sub>@CS@Dex (MCD, chitosan (CS)-modified molybdenum disulfide (MoS<sub>2</sub>) loaded with anti-inflammatory disulfide (Dex)), which significantly increased the intra-articular drug release efficiency in OA joints with the satisfactory photothermal conversion efficiency of the drug carrier [95]. In general reaction process shown in Figures 10(A-B), after injection of the nanoparticles and under the NIR infrared illumination, drugs loaded in the MCD are released in the inflamed areas and induce activated macrophage, which further results in reduction of inflammatory factors to realize the treatment goals. The photothermal properties and photoacoustic signals fluctuations shown in Figures 10(C-F) suggest that the MCD has a sound photothermal conversion ability and its long retaining period in OA joints helps to maintain an efficient drug release. Semiquantitative results shown in Figures 10(G-I) further confirm that the MCD, as an efficient photothermal contrast and drug carrier, can yield therapeutic outcomes superior to other treatment methods.

## Clinical application

Sun *et al.* reported *in vivo* detection of OA in the finger joints via three-dimensional (3D) quantitative photoacoustic tomography (PAT) [96, 97], which uses a reconstruction algorithm to obtain absorption

coefficient images of the joints. As illustrated in Figures 11(A-B), different sections, including both coronal and sagittal sections, of the fingers were imaged by the PAT. As seen, it might be hard to tell the structure difference between the healthy and OA joints from the PAT recovered 3D images, but they do show that the absorption coefficient has larger variations at different imaging depths for the OA finger joint cavity (Figures 11D and F), while for the healthy joint cavity the PA signals keep relatively constant at different depths (Figures 11C and E). It also can be found from the quantitative results that the space between joints also exhibits apparent differences for the OA and healthy joints. Similar observations have been reported from two-dimensional (2D) quantitative PA imaging with the same system proposed by this group, confirming the depth-dependent feature of tissue absorption coefficient for OA joints [98]. They also founded that the functional parameters changes in OA joints compared with normal human fingers [81], as mentioned in Figure 5.

The tissue absorption spectra, as reflected by the PA signal intensity changes as a function of optical wavelength, corresponding to cartilages of different degrees of damage has also been investigated. Wu *et al.* used the PA spectra changes to differentiate the damage degree of cartilages, and the results are shown in Figure 12 [99]. As seen, for the least

damaged cartilage in the wavelength range from 500 nm to 1300 nm, there are two absorption peaks at 980 and 1185 nm, which are associated with the absorption peaks of water and collagen, respectively. But the spectrum profile changes with the degree of damage. It is hard to find the two above-mentioned absorption peaks in most damaged cartilage, suggesting a loss of balance between the water and collagen contents inside the damaged cartilage. Moreover, the elevated absorption around 550 nm for most damaged cartilage confirms the increased vascularization of OA as illustrated in Figures 2 and 4.

## Conclusion and perspectives

In this manuscript, we have narratively reviewed the applications of photothermal effects in the diagnosis and treatment of OA. Regarding diagnosis, photoacoustic imaging, a hybrid noninvasive imaging modality that integrates the advantages of optical (absorption) contrast with ultrasound detection, is considered. The working principle of PA imaging and current studies in cancers and brain activities are first described, which is followed by a summarization of its applications for

diagnosis and status evaluation of OA joints from structural changes, functional parameters, as well as molecular information. With PA imaging, it is feasible to capture the structural changes in spongy bone and cartilage, allowing one to identify OA joints from normal joints. Functional parameters, including vascularity, oxygen saturation, hemoglobin concentration, water contents, acoustic velocities, and viscoelasticity, experience considerable variations even in the early stage of OA joints, which further causes changes of the optical spectra. Thus, it is possible to achieve early diagnosis and developmental stage evaluation of the OA disease with the assist of PA imaging. Moreover, PA can also be used to sense and then quantify the changes of molecular information. For example, the glycosaminoglycans concentration, an important indicator of the cartilage denegation degree, can be captured by PA with specifically designed nanoprobes. Collectively, with the capability of structural, functional, and molecular imaging, PA provides a promising tool for early-stage detection and timely treatment of OA.

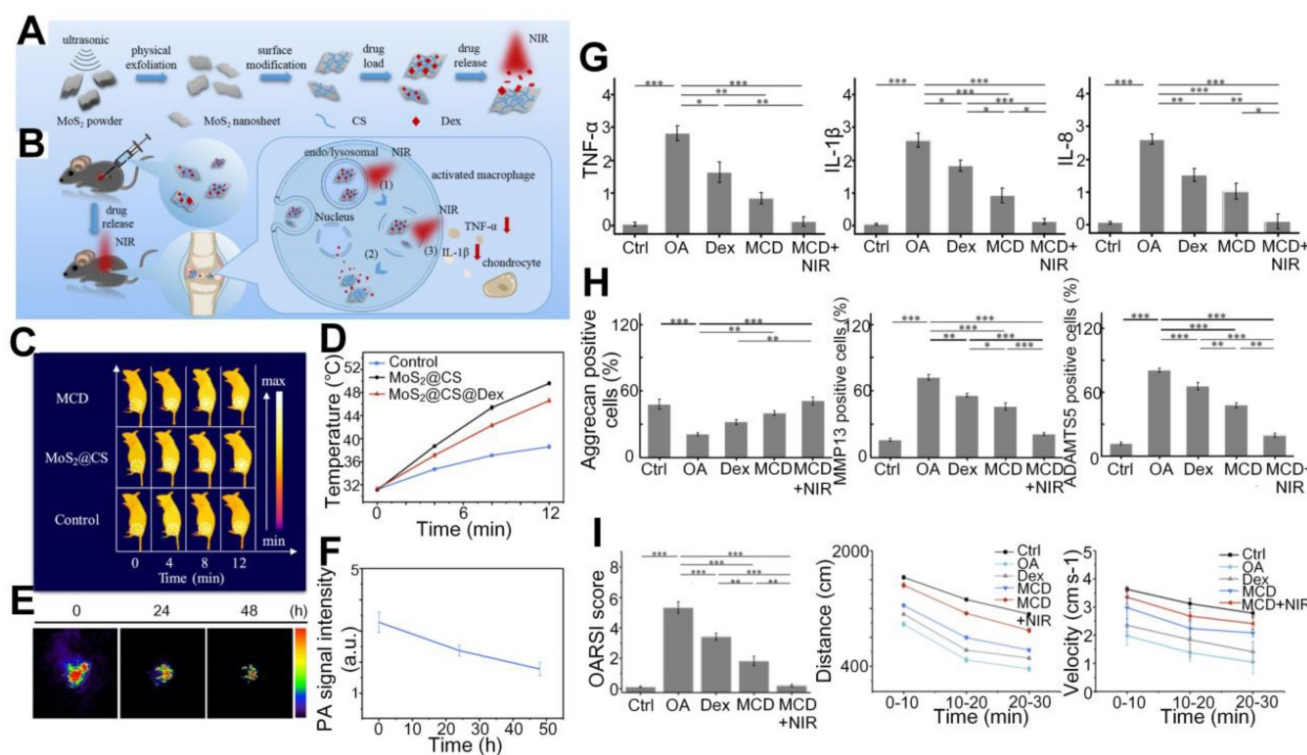


**Figure 10.** (A) - (B) Schematic diagram of the synthesization and reaction process of the MCD nanoparticles. (C) - (F) Photothermal effect and remaining time duration of the MCD in mouse joints. (G) - (I) Semiquantitative comparisons of inflammatory factors (TNF- $\alpha$ , IL-1 $\beta$ , and IL-8), therapy outcomes (three proteins associated with OA pathology and cartilage reconstruction), composite scores, movement distance, and velocity in OA joints among different treatment methods. Figures adapted with permission from Ref. [95]. Copyright © 2019, American Chemical Society.

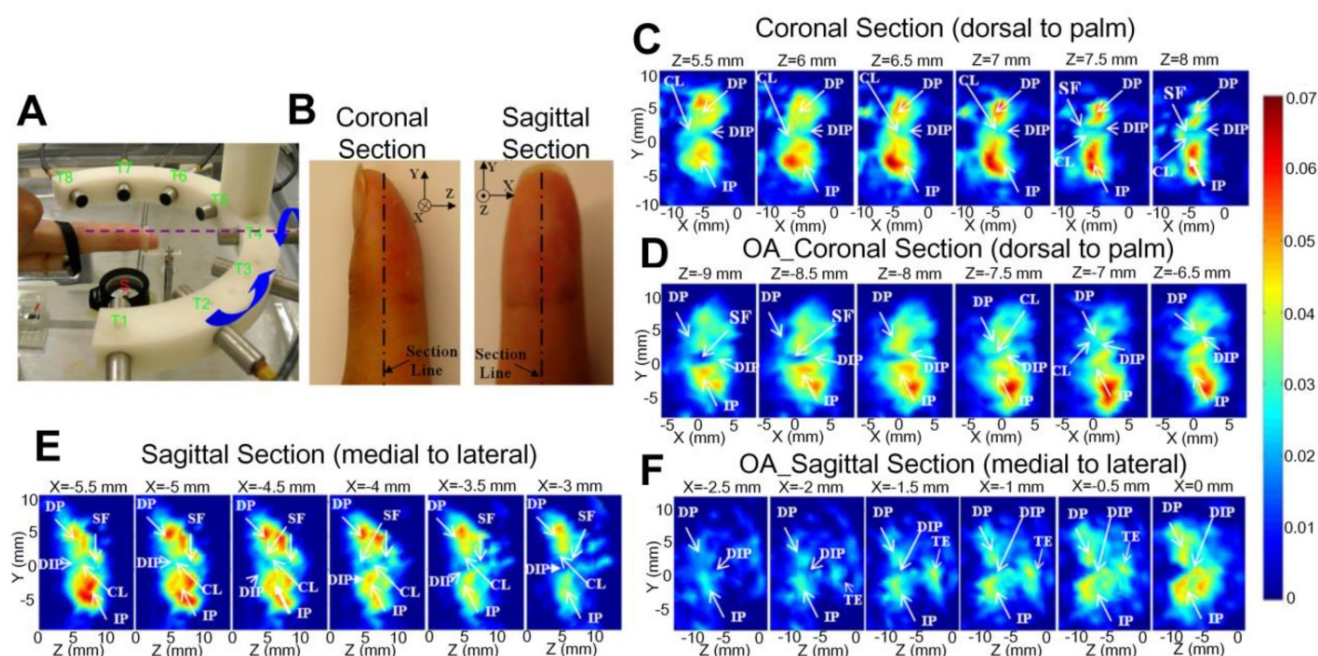


**Figure 11.** (A) Photograph of the PAT system. (B) Photograph of the finger joint through different sections. (C)-(D) PA recovered 3D absorption coefficient image of the corona section for normal and OA joints, respectively. (E)-(F) PA recovered 3D absorption coefficient image of the sagittal section for normal and OA joints, respectively. CL: cartilage; DIP: distal interphalangeal joint; DP: distal phalanx; IP: intermediate phalanx; SF: synovial fluid. Figures adapted with permission from Ref. [96]. Copyright © 2011, American Association of Physicists in Medicine.

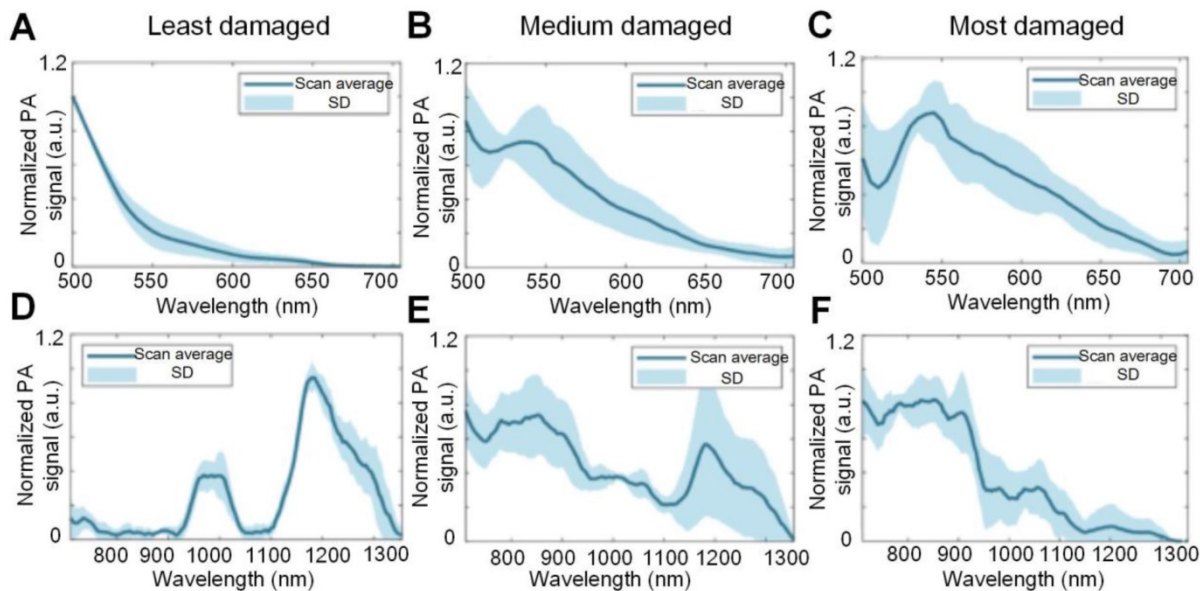


**Figure 12.** (A)-(C) PA spectra of different damaged cartilage (least damaged, medium damaged and most damaged) at 500 nm- 700 nm. (D)-(F) PA spectra of different damaged cartilage (least damaged, medium damaged and most damaged) at 710 nm- 1300 nm. Figures adapted with permission from Ref. [99]. Copyright © 1969, Elsevier (1969).

Regarding the treatment of OA, PTT is reviewed in this work. As a relatively new therapeutic technology, PTT has seen wide applications in cancer treatment but only a few in OA joints treatment. But the noninvasive feature and confirmed enhanced therapeutic ability of PTT have made it distinctively potential for the treatment of OA joints treatment. Moreover, the therapeutic precision, efficiency, and recovery outcomes can be further enhanced with the help of molecule-targeted contrast agents. Lastly, the

relevant clinical applications including analyzing changes in tissue absorption coefficient and absorption spectrum associated with human OA have been discussed.

That said, at current stage the clinical trials of PA and PTT in OA diagnosis or treatments are yet limited within a shallow penetration depth (e.g., finger) in human body, and the research models are mainly aiming at animals. Taking consideration of the trade-off between penetration depth and spatial

resolution, how to achieve high resolution and deep penetration simultaneously so that PA imaging can be extended for clinics is an important challenge, which holds great significances in clinical diagnosis for OA and many other diseases.

There are two potential strategies to tackle the challenge. One is to explore if the diffusive light at depths in joints can be refocused so as to enhance the *in-situ* photon flux and hence the PA signal strength. Note that PA imaging has indeed reduced the influence of optical scattering by converting light, diffused or not diffused, into non-scattered ultrasonic waves due to optical absorption, which, however, only applies to the signal detection aspect. For the generation of signals, the amount of photons reaching the region of interest that can be absorbed and converted into heat and hence the effective penetration depth in PA are still throttled by the strong scattering in the tissue. Optical wavefront shaping can compensate for the scattering-induced phase distortion of light and generate optical focusing through or within a highly scattering medium [100, 101]. Especially, when photoacoustic signal is used the guidestar for optimization [102], acoustical- or even optical-diffraction limited light focusing may be achieved at the focal position of the ultrasound transducer at depths in tissue, which can significantly enhance the signal strength and hence the penetration depth. The feasibility of such a concept of photoacoustically guided wavefront shaping for enhanced photoacoustic imaging has already been demonstrated in tissue-mimicking phantom and ex-vivo tissue [100, 103, 104], and it is currently under development towards in-vivo applications. Once it is mature, it will allow more reliable PA diagnosis of OA even at depths. The other possible solution is applying deep learning to achieve enhanced PA resolution in deeper tissue regions. Deep learning has seen wide applications in bioimaging including PA imaging in recent years due to its excellence in achieving super resolution imaging [105-107]. For example, in PA imaging, deep learning assistance has enabled 100% decrease in background noise and up to 250% increase in signal strength [108]. Moreover, the trained network has the capability to intelligently highlight the target and reduce the fuzzy information via big data learning. Currently, the state-of-art PACT has been successfully applied to human breast and brain trials *in vivo* [18, 109], albeit with limited resolution. In application, the neural network can be designed and trained based on co-registered low-resolution PACT and high-resolution PAM data acquired from OA joints in relatively shallow tissue regions. Then, the transformation capability of the network can be extended to deep tissue regions that

only allows for PACT, producing high-resolution PA images of OA joints that cannot be physically obtained with existing PA implementations.

Apart from the penetration depth, the sensitivity of existing nanoprobe could be further improved to enhance the detection sensitivity and specificity. Current nanoprobe as the photoacoustic or photothermal contrasts mostly conjugate to the OA regime passively via permeability or microenvironment variations. These nanoparticles may also gather in the surrounding regions, reducing the contrast, precision, or the efficiency of photoacoustic diagnosis or photothermal-triggered treatment. If key molecules for early OA can be identified and active targeting probes can be synthesized, PA can potentially precisely locate the lesion of early OA, which can also considerably increase the treatment efficiency through photothermal-triggered therapy while minimizing the damage to surrounding normal tissues. Since PA and PTT share the same photothermal mechanism, it is feasible to integrate these two modules into one system that can achieve precise detection of early-stage OA joints with PA and timely treatment with PTT simultaneously, providing a promising theranostic platform for OA joints.

On the other side, the natural cavity structure of human joints provides another opportunity for PA imaging to bypass the technical challenges of tissue penetration depth to achieve high-resolution information down to the molecular level. The joint cavity is alike in hollow structure in the cardiovascular and gastrointestinal systems. In this regard, nanorobots can be further developed for the human joint based on photoacoustic endoscopy (PAE) for blood vessels [110] and the digestive tract [111]. By doing so, we might be able to overcome the obstacles in the transmission of sound waves to achieve micron-level resolution at millimeter-level imaging depths. Moreover, the imaging nanorobots shall be designed for specific imaging objects and imaging ranges with the multimodal functional system. It would be better at finding the location of the lesion timely, providing the doctor with images of the lesion area, guiding the operation, monitoring, collecting specimens, and removing the location of the lesion inside osteoarthritic joint at its early stage of disease.

Although there have been quite a few attempts to deploy PA for OA imaging, the majority of these studies remain limited to proof-of-concept in the laboratory setting. Some nano-contrast agents for PA molecular imaging play a role in OA diagnosis, nevertheless, there are still many issues to be further addressed before clinical translation, such as their immunogenicity, toxicity, particle size, *etc.* Among 49

clinical trials related to PA technology in the ClinicalTrials.gov database, there are only two ongoing clinical trials for rheumatoid arthritis (one in China [112], another one in the United States [113]) but none for OA. Although there is still a long way ahead, PA holds a good promise for clinical translation. It prompts the needs for joint efforts among engineers, clinicians and their industrial partners along this direction.

In conclusion, PA imaging technology can not only perform specific structure imaging of tissues with high resolution and high contrast, identify specific components in tissues, but also can combine molecular nanorobots for targeted imaging, showing huge potential clinical market value. It has great economic value and social significance, promoting the further clinical transformation and industrialization of PA imaging technology in OA theranostic. We hope this mini review can provide a better understanding of the diagnosis and treatment of OA with exciting innovations based on tissue photothermal effects. It may also inspire more explorations in the field towards earlier and better theranostic of OA.

## Abbreviations

OA: osteoarthritis; X-ray: radiography; PET: positron emission tomography; MRI: magnetic resonance imaging; OCT: optical coherence tomography; US: ultrasound; JSW: joint space width; JNS: joint space narrowing; SPECT: single-photon emission computed tomography; PA: photoacoustic; PAM: photoacoustic microscopy; PACT: photoacoustic computed tomography; SNR: signal-to-noise ratio; PTT: photothermal therapy; MMPs: matrix metalloproteinases; NO: nitric oxide; ROS: reactive oxygen species; TNF- $\alpha$ : tumour necrosis factor- $\alpha$ ; IL-1 $\beta$ : interleukin-1 $\beta$ ; PD: power doppler; DMM: medial meniscus; HbO<sub>2</sub>: oxyhemoglobin; Hb: deoxyhemoglobin; DIP: distal interphalangeal; SERS: surface-enhanced Raman scattering; LIPA: laser-induced PA; GAGs: glycosaminoglycan; PLL-MNPs: poly-L-lysine-encapsulated melanin nanoparticles; MNP: melanin nanoparticles; HA: hyaluronic acid; NHsPP: NO-Hb@siRNA@PLGA-PEG; MCD: MoS<sub>2</sub>@CS@Dex; CS: chitosan; MoS<sub>2</sub>: molybdenum disulfide; Dex: disulfide; 3D: three-dimensional; PAT: photoacoustic tomography; 2D: two-dimensional; PAE: photoacoustic endoscopy.

## Acknowledgements

This work was partially supported by the National Natural Science Foundation of China (NSFC) (81930048, 81627805), Hong Kong Innovation and Technology Commission (GHP/043/19SZ, GHP/044/19GD, MHP/011/20), Hong Kong Research

Grant Council (15217721, R5029-19, 25100818, 15106120, 15100821), Guangdong Science and Technology Commission (2019BT02X105, 2019A1515011374), Hong Kong Health and Medical Research Fund (01150087, 16172691), NFSC/RGC schemes (N\_PolyU 520/20), and the Hong Kong Polytechnic University Project of Strategic Importance (ZE2C).

## Competing Interests

The authors have declared that no competing interest exists.

## References

- Zhang YQ, Jordan JM. Epidemiology of osteoarthritis. *Clin Geriatr Med.* 2010; 26: 355-69.
- Simon TM, Jackson DW. Articular cartilage: injury pathways and treatment options. *Sports Med Arthrosc.* 2018; 26: 31-9.
- Dieppe PA, Lohmander LS. Pathogenesis and management of pain in osteoarthritis. *Lancet.* 2005; 365: 965-73.
- Braun HJ, Gold GE. Diagnosis of osteoarthritis: imaging. *Bone.* 2012; 51: 278-88.
- Roemer FW, Demehri S, Omoumi P, Link TM, Kijowski R, Saarakkala S, et al. State of the Art: Imaging of Osteoarthritis-Revisited 2020. *Radiology.* 2020; 296: 5-21.
- Wang X, Oo WM, Linklater JM. What is the role of imaging in the clinical diagnosis of osteoarthritis and disease management? *Rheumatology (Oxford).* 2018; 57: iv51-iv60.
- Beard P. Biomedical photoacoustic imaging. *Interface Focus.* 2011; 1: 602-31.
- Xu MH, Wang LHV. Photoacoustic imaging in biomedicine. *Rev Sci Instrum.* 2006; 77.
- Zhou YY, Chen JB, Liu C, Liu CB, Lai PX, Wang LD. Single-shot linear dichroism optical-resolution photoacoustic microscopy. *Photoacoustics.* 2019; 16: 100148.
- Zhou YY, Cao F, Li HH, Huang XZ, Wei DS, Wang LD, et al. Photoacoustic imaging of microenvironmental changes in facial cupping therapy. *Biomed Opt Express.* 2020; 11: 2394-401.
- Wang LHV, Hu S. Photoacoustic tomography: *in vivo* imaging from organelles to organs. *Science.* 2012; 335: 1458-62.
- Luke GP, Nam SY, Emelianov SY. Optical wavelength selection for improved spectroscopic photoacoustic imaging. *Photoacoustics.* 2013; 1: 36-42.
- Luke GP, Yeager D, Emelianov SY. Biomedical applications of photoacoustic imaging with exogenous contrast agents. *Ann Biomed Eng.* 2012; 40: 422-37.
- Xu J, Cheng X, Chen F, Li W, Xiao X, Lai P, et al. Fabrication of multifunctional polydopamine-coated gold nanobones for PA/CT imaging and enhanced synergistic chemo-photothermal therapy. *J Mater Sci Technol.* 2021; 63: 97-105.
- Wang SS, Chen RH, Yu Q, Huang WC, Lai PX, Tang JX, et al. Near-infrared plasmon-boosted heat/oxygen enrichment for reversing rheumatoid arthritis with metal/semiconductor composites. *ACS Appl Mater Inter.* 2020; 12: 45796-806.
- Huang XZ, Zhou YY, Woo CM, Pan Y, Nie LM, Lai PX. Multifunctional layered black phosphorene-based nanoplatform for disease diagnosis and treatment: a review. *Front Optoelectron.* 2020; 13: 327-51.
- Wong TITW, Zhang RY, Hai PF, Zhang C, Pleitez MA, Aft RL, et al. Fast label-free multilayered histology-like imaging of human breast cancer by photoacoustic microscopy. *Sci Adv.* 2017; 3.
- Lin L, Hu P, Shi JH, Appleton CM, Maslov K, Li L, et al. Single-breath-hold photoacoustic computed tomography of the breast. *Nat Commun.* 2018; 9.
- Yao J, Wang L, Yang J-M, Maslov KL, Wong TT, Li L, et al. High-speed label-free functional photoacoustic microscopy of mouse brain in action. *Nat Methods.* 2015; 12: 407-10.
- Valluru KS, Willmann JK. Clinical photoacoustic imaging of cancer. *Ultrasonography.* 2016; 35: 267-80.
- Qi S, Zhang YC, Liu GY, Chen JB, Li XZ, Zhu Q, et al. Plasmonic-doped melanin-mimic for CXCR4-targeted NIR-II photoacoustic computed tomography-guided photothermal ablation of orthotopic hepatocellular carcinoma. *Acta Biomater.* 2021; 129: 245-57.
- Huang X, Shang W, Deng H, Zhou Y, Cao F, Fang C, et al. Clothing spiny nanoprobes against the mononuclear phagocyte system clearance *in vivo*: Photoacoustic diagnosis and photothermal treatment of early stage liver cancer with erythrocyte membrane-camouflaged gold nanostars. *Appl Mater Today.* 2019.
- Yang X, Chen YH, Xia F, Sawan M. Photoacoustic imaging for monitoring of stroke diseases: A review. *Photoacoustics.* 2021; 23: 100287.
- Cao F, Qiu Z, Li H, Lai P. Photoacoustic imaging in oxygen detection. *Appl Sci.* 2017; 7: 1262.
- Yao JJ, Wang LHV. Photoacoustic brain imaging: from microscopic to macroscopic scales. *Neurophotonics.* 2014; 1.

26. Liu YJ, Liu HH, Yan HX, Liu YC, Zhang JS, Shan WJ, et al. Aggregation-induced absorption enhancement for deep near-infrared II photoacoustic imaging of brain gliomas *in vivo*. *Adv Sci*. 2019; 6.
27. Jo J, Lee CH, Kopelman R, Wang XD. *In vivo* quantitative imaging of tumor pH by nanosonophore assisted multispectral photoacoustic imaging. *Nat Commun*. 2017; 8.
28. Yang K, Zhang S, Zhang G, Sun X, Lee ST, Liu Z. Graphene in mice: ultrahigh *in vivo* tumor uptake and efficient photothermal therapy. *Nano Lett*. 2010; 10: 3318-23.
29. Chen X, Liu Y, Wen Y, Yu Q, Liu J, Zhao Y, et al. A photothermal-triggered nitric oxide nanogenerator combined with siRNA for precise therapy of osteoarthritis by suppressing macrophage inflammation. *Nanoscale*. 2019; 11: 6693-709.
30. Guo B, Sheng Z, Hu D, Liu C, Zheng H, Liu B. Through Scalp and Skull NIR-II Photothermal Therapy of Deep Orthotopic Brain Tumors with Precise Photoacoustic Imaging Guidance. *Adv Mater*. 2018; 30: e1802591.
31. Wei WF, Zhang XY, Zhang S, Wei G, Su ZQ. Biomedical and bioactive engineered nanomaterials for targeted tumor photothermal therapy: A review. *Mater Sci Eng C Mater Biol Appl*. 2019; 104.
32. Dai H, Shen Q, Shao J, Wang W, Gao F, Dong X. Small molecular NIR-II fluorophores for cancer phototheranostics. *The Innovation*. 2021; 2: 100082.
33. Barbour KE, Helmick CG, Theis KA, Murphy LB, Hootman JM, Brady TJ, et al. Prevalence of doctor-diagnosed arthritis and arthritis-attributable activity limitation—United States, 2010–2012. *MMWR Morb Mortal Wkly Rep*. 2013; 62: 869.
34. Palazzo C, Nguyen C, Lefevre-Colau M-M, Rannou F, Poiraudou S. Risk factors and burden of osteoarthritis. *Ann Phys Rehabil Med*. 2016; 59: 134-8.
35. Jiang L, Zhu X, Rong J, Xing B, Wang S, Liu A, et al. Obesity, osteoarthritis and genetic risk: The rs182052 polymorphism in the ADIPOQ gene is potentially associated with risk of knee osteoarthritis. *Bone Joint Res*. 2018; 7: 494-500.
36. He Y, Li Z, Alexander PG, Ocasio-Nieves BD, Yocum L, Lin H, et al. Pathogenesis of osteoarthritis: risk factors, regulatory pathways in chondrocytes, and experimental models. *Biology (Basel)*. 2020; 9: 194.
37. Akkiraju H, Nohe A. Role of chondrocytes in cartilage formation, progression of osteoarthritis and cartilage regeneration. *J Dev Biol*. 2015; 3: 177-92.
38. Maldonado M, Nam J. The role of changes in extracellular matrix of cartilage in the presence of inflammation on the pathology of osteoarthritis. *Biomed Res Int*. 2013; 2013: 284873-.
39. Goldring SR, Goldring MB. Changes in the osteochondral unit during osteoarthritis: structure, function and cartilage–bone crosstalk. *Nat Rev Rheumatol*. 2016; 12: 632-44.
40. Felson DT. Epidemiology of hip and knee osteoarthritis. *Epidemiol Rev*. 1988; 10: 1-28.
41. Haara M, Manninen P, Kröger H, Arokoski J, Kärkkäinen A, Knekt P, et al. Osteoarthritis of finger joints in Finns aged 30 or over: prevalence, determinants, and association with mortality. *Ann Rheum Dis*. 2003; 62: 151-8.
42. Gellhorn AC, Katz JN, Suri P. Osteoarthritis of the spine: the facet joints. *Nat Rev Rheumatol*. 2013; 9: 216-24.
43. Loeser RF, Goldring SR, Scanzello CR, Goldring MB. Osteoarthritis: a disease of the joint as an organ. *Arthritis Rheum*. 2012; 64: 1697-707.
44. Makris EA, Hadidi P, Athanasiou KA. The knee meniscus: structure–function, pathophysiology, current repair techniques, and prospects for regeneration. *Biomaterials*. 2011; 32: 7411-31.
45. Hada S, Kaneko H, Sadatsuki R, Liu L, Futami I, Kinoshita M, et al. The degeneration and destruction of femoral articular cartilage shows a greater degree of deterioration than that of the tibial and patellar articular cartilage in early stage knee osteoarthritis: a cross-sectional study. *Osteoarthritis Cartilage*. 2014; 22: 1583-9.
46. Pearle AD, Warren RF, Rodeo SA. Basic science of articular cartilage and osteoarthritis. *Clin Sports Med*. 2005; 24: 1-12.
47. Mankin HJ. The response of articular cartilage to mechanical injury. *J Bone Joint Surg*. 1982; 64: 460-6.
48. van der Sluijs JA, Geesink RG, van der Linden AJ, Bulstra SK, Kuyper R, Drukker J. The reliability of the Mankin score for osteoarthritis. *J Orthop Res*. 1992; 10: 58-61.
49. Li G, Yin J, Gao J, Cheng TS, Pavlos NJ, Zhang C, et al. Subchondral bone in osteoarthritis: insight into risk factors and microstructural changes. *Arthritis Res Ther*. 2013; 15: 1-12.
50. Castañeda S, Roman-Blas JA, Largo R, Herrero-Beaumont G. Subchondral bone as a key target for osteoarthritis treatment. *Biochem Pharmacol*. 2012; 83: 315-23.
51. Intema F, Hazewinkel HA, Gouwens D, Bijlsma JW, Weinans H, Laferte FP, et al. In early OA, thinning of the subchondral plate is directly related to cartilage damage: results from a canine ACLT-menisectomy model. *Osteoarthritis Cartilage*. 2010; 18: 691-8.
52. Buckland-Wright C. Subchondral bone changes in hand and knee osteoarthritis detected by radiography. *Osteoarthritis Cartilage*. 2004; 12 Suppl A: S10-9.
53. Buckland-Wright JC, Messent EA, Bingham CO, 3rd, Ward RJ, Tonkin C. A 2 yr longitudinal radiographic study examining the effect of a bisphosphonate (risedronate) upon subchondral bone loss in osteoarthritic knee patients. *Rheumatology (Oxford)*. 2007; 46: 257-64.
54. Li J, Xue J, Jing Y, Wang M, Shu R, Xu H, et al. SOST deficiency aggravates osteoarthritis in mice by promoting sclerosis of subchondral bone. *Biomed Res Int*. 2019; 2019: 7623562.
55. Frobell RB. Change in cartilage thickness, posttraumatic bone marrow lesions, and joint fluid volumes after acute ACL disruption: a two-year prospective MRI study of sixty-one subjects. *J Bone Joint Surg Am*. 2011; 93: 1096-103.
56. McDermott I, Amis A. The consequences of meniscectomy. *J Bone Joint Surg Br*. 2006; 88: 1549-56.
57. Guermazi A, Niu J, Hayashi D, Roemer FW, Englund M, Neogi T, et al. Prevalence of abnormalities in knees detected by MRI in adults without knee osteoarthritis: population based observational study (Framingham Osteoarthritis Study). *Polym Int*. 2012; 345: e5339.
58. Walsh DA, McWilliams DF, Turley MJ, Dixon MR, Fransès RE, Mapp PI, et al. Angiogenesis and nerve growth factor at the osteochondral junction in rheumatoid arthritis and osteoarthritis. *Rheumatology*. 2010; 49: 1852-61.
59. Houard X, Goldring MB, Berenbaum F. Homeostatic mechanisms in articular cartilage and role of inflammation in osteoarthritis. *Curr Rheumatol Rep*. 2013; 15: 375.
60. Calvo E, Palacios I, Delgado E, Sánchez-Pernaute O, Largo R, Egido J, et al. Histopathological correlation of cartilage swelling detected by magnetic resonance imaging in early experimental osteoarthritis. *Osteoarthritis Cartilage*. 2004; 12: 878-86.
61. Heinegård D, Saxne T. The role of the cartilage matrix in osteoarthritis. *Nat Rev Rheumatol*. 2011; 7: 50-6.
62. Riegger J, Brenner RE. Pathomechanisms of posttraumatic osteoarthritis: chondrocyte behavior and fate in a precarious environment. *Int J Mol Sci*. 2020; 21: 1560.
63. Kapoor M, Martel-Pelletier J, Lajeunesse D, Pelletier J-P, Fahmi H. Role of proinflammatory cytokines in the pathophysiology of osteoarthritis. *Nat Rev Rheumatol*. 2011; 7: 33-42.
64. Hu W, Chen Y, Dou C, Dong S. Microenvironment in subchondral bone: predominant regulator for the treatment of osteoarthritis. *Ann Rheum Dis*. 2021; 80: 413-22.
65. Hunter DJ, Bierma-Zeinstra S. Osteoarthritis. *Lancet*. 2019; 393: 1745-59.
66. Suri S, Gill SE, Massena de Camin S, Wilson D, McWilliams DF, Walsh DA. Neurovascular invasion at the osteochondral junction and in osteophytes in osteoarthritis. *Ann Rheum Dis*. 2007; 66: 1423-8.
67. Saito M, Sasho T, Yamaguchi S, Ikegawa N, Akagi R, Muramatsu Y, et al. Angiogenic activity of subchondral bone during the progression of osteoarthritis in a rabbit anterior cruciate ligament transection model. *Osteoarthritis Cartilage*. 2012; 20: 1574-82.
68. Su W, Liu G, Liu X, Zhou Y, Sun Q, Zhen G, et al. Angiogenesis stimulated by elevated PDGF-BB in subchondral bone contributes to osteoarthritis development. *JCI Insight*. 2020; 5.
69. Zhen G, Wen C, Jia X, Li Y, Crane JL, Mears SC, et al. Inhibition of TGF- $\beta$  signaling in mesenchymal stem cells of subchondral bone attenuates osteoarthritis. *Nat Med*. 2013; 19: 704-12.
70. Hu Y, Chen X, Wang S, Jing Y, Su J. Subchondral bone microenvironment in osteoarthritis and pain. *Bone Res*. 2021; 9: 1-13.
71. Mansell JP, Collins C, Bailey AJ. Bone, not cartilage, should be the major focus in osteoarthritis. *Nat Clin Pract Rheumatol*. 2007; 3: 306-7.
72. Bailey AJ, Mansell JP, Sims TJ, Banske X. Biochemical and mechanical properties of subchondral bone in osteoarthritis. *Biorheology*. 2004; 41: 349-58.
73. Karlas A, Pleitez MA, Aguirre J, Ntziachristos V. Photoacoustic imaging in endocrinology and metabolism. *Nat Rev Endocrinol*. 2021; 17: 323-35.
74. Liu W, Zhang HF. Photoacoustic imaging of the eye: A mini review. *Photoacoustics*. 2016; 4: 112-23.
75. Nyayapathi N, Xia J. Photoacoustic imaging of breast cancer: a mini review of system design and image features. *J Biomed Opt*. 2019; 24: 121911.
76. Mallidi S, Luke GP, Emelianov S. Photoacoustic imaging in cancer detection, diagnosis, and treatment guidance. *Trends Biotechnol*. 2011; 29: 213-21.
77. Izumi T, Sato M, Yabe Y, Hagiwara Y, Saijo Y. Ultrasonic and photoacoustic imaging of knee joints in normal and osteoarthritis rats. *IEEE Eng Med Bio*. 2013; 1116-9.
78. Izumi T, Sato M, Hagiwara Y, Saijo Y. Photoacoustic imaging of rat knee joint. *IEEE Int Ultra Sym*. 2012: 1417-20.
79. Hagiwara Y, Izumi T, Yabe Y, Sato M, Sonofuchi K, Kanazawa K, et al. Simultaneous evaluation of articular cartilage and subchondral bone from immobilized knee in rats by photoacoustic imaging system. *J Orthop Sci*. 2015; 20: 397-402.
80. Liu Z, Au M, Wang X, Chan PB, Lai P, Sun L, et al. Photoacoustic imaging of synovial tissue hypoxia in experimental post-traumatic osteoarthritis. *Prog Biophys Mol Biol*. 2019; 148: 12-20.
81. Xiao JY, He JS. Multispectral quantitative photoacoustic imaging of osteoarthritis in finger joints. *Appl Opt*. 2010; 49: 5721-7.
82. Sun Y, Sobel E, Jiang H. Noninvasive imaging of hemoglobin concentration and oxygen saturation for detection of osteoarthritis in the finger joints using multispectral three-dimensional quantitative photoacoustic tomography. *J Opt*. 2013; 15.
83. Yuan Z, Xiao J, Sun Y, Sobel ES, He JS, Jiang HB. Image-guided photoacoustic spectroscopy in diagnosis of osteoarthritis in hands: an initial study. *Photonics Therapeutics and Diagnostics VII*. 2011; 7883.
84. Li Q, Ge X, Ye J, Li Z, Su L, Wu Y, et al. Dual ratiometric SERS and photoacoustic core-satellite nanoprobe for quantitatively visualizing hydrogen peroxide in inflammation and cancer. *Angew Chem Int Ed Engl*. 2021; 60: 7323-32.

85. Ye J, Li Z, Fu Q, Li Q, Zhang X, Su L, et al. Quantitative photoacoustic diagnosis and precise treatment of inflammation *in vivo* using activatable theranostic nanoprobe. *Adv Funct Mater.* 2020; 30.
86. Ishihara M, Sato M, Kaneshiro N, Mitani G, Sato S, Mochida J, et al. Development of a diagnostic system for osteoarthritis using a photoacoustic measurement method. *Laser Surg Med.* 2006; 38: 249-55.
87. Sato M, Ishihara M, Furukawa K, Kaneshiro N, Nagai T, Mitani G, et al. Recent technological advancements related to articular cartilage regeneration. *Med Biol Eng Comput.* 2008; 46: 735-43.
88. Ishihara M, Sato M, Sato S, Kikuchi T, Ishihara M, Mochida J, et al. Applicability of photoacoustic measurement for biomechanical characterization: From *in vitro* engineered tissue characterization to *in vivo* diagnosis. *Laser Interaction with Tissue and Cells Xv.* 2004; 5319: 11-4.
89. Ishihara M, Sato M, Sato S, Kikuchi T, Mochida J, Kikuchi M. Usefulness of photoacoustic measurements for evaluation of biomechanical properties of tissue-engineered cartilage. *Tissue Eng.* 2005; 11: 1234-43.
90. Sato M, Yamato M, Mitani G, Takagaki T, Hamahashi K, Nakamura Y, et al. Combined surgery and chondrocyte cell-sheet transplantation improves clinical and structural outcomes in knee osteoarthritis. *Npj Regen Med.* 2019; 4.
91. Ukai T, Sato M, Ishihara M, Yokoyama M, Takagaki T, Mitani G, et al. Usefulness of using laser-induced photoacoustic measurement and 3.0 Tesla MRI to assess knee cartilage damage: a comparison study. *Arthritis Res Ther.* 2015; 17: 383.
92. Chen L, Ji Y, Hu X, Cui C, Liu H, Tang Y, et al. Cationic poly-L-lysine-encapsulated melanin nanoparticles as efficient photoacoustic agents targeting to glycosaminoglycans for the early diagnosis of articular cartilage degeneration in osteoarthritis. *Nanoscale.* 2018; 10: 13471-84.
93. Xiao S, Tang Y, Lin Y, Lv Z, Chen L. Tracking Osteoarthritis Progress through Cationic Nanoprobe-Enhanced Photoacoustic Imaging of Cartilage. *Acta Biomater.* 2020; 109: 153-62.
94. Zhao C, Chen J, Ye J, Li Z, Su L, Wang J, et al. Structural transformative antioxidants for dual-responsive anti-inflammatory delivery and photoacoustic inflammation imaging. *Angew Chem Int Ed Engl.* 2021; 60: 14458-66.
95. Zhao Y, Wei C, Chen X, Liu J, Yu Q, Liu Y, et al. Drug Delivery System Based on Near-Infrared Light-Responsive Molybdenum Disulfide Nanosheets Controls the High-Efficiency Release of Dexamethasone To Inhibit Inflammation and Treat Osteoarthritis. *ACS Appl Mater Interfaces.* 2019; 11: 11587-601.
96. Sun Y, Sobel ES, Jiang HB. First assessment of three-dimensional quantitative photoacoustic tomography for *in vivo* detection of osteoarthritis in the finger joints. *Med Phys.* 2011; 38: 4009-17.
97. Sun Y, Sobel E, Jiang HB. *In vivo* detection of osteoarthritis in the hand with three-dimensional photoacoustic tomography. *Photonics Therapeutics and Diagnostics Vi.* 2010; 7548.
98. Xiao JY, Yao L, Sun Y, Sobel ES, He JS, Jiang HB. Quantitative two-dimensional photoacoustic tomography of osteoarthritis in the finger joints. *Opt Express.* 2010; 18: 14359-65.
99. Wu M, van Teeffelen BCJ, Ito K, van de Vosse FN, Janssen RPA, van Donkelaar CC, et al. Spectroscopic photoacoustic imaging of cartilage damage. *Osteoarthritis Cartilage.* 2021; 29: 1071-80.
100. Yu ZP, Li HH, Lai PX. Wavefront shaping and its application to enhance photoacoustic imaging. *Appl Sci (Basel).* 2017; 7.
101. Conkey DB, Caravaca-Aguirre AM, Dove JD, Ju HY, Murray TW, Piestun R. Super-resolution photoacoustic imaging through a scattering wall. *Nat Commun.* 2015; 6.
102. Lai P, Wang L, Tay JW, Wang LV. Photoacoustically guided wavefront shaping for enhanced optical focusing in scattering media. *Nat Photonics.* 2015; 9: 126-32.
103. Lai PX, Wang LD, Tay JW, Wang LHV. Photoacoustically guided wavefront shaping for enhanced optical focusing in scattering media. *Nat Photonics.* 2015; 9: 126-32.
104. Tay JW, Lai PX, Suzuki Y, Wang LV. Ultrasonically encoded wavefront shaping for focusing into random media. *Sci Rep.* 2014; 4.
105. Wang H, Rivenson Y, Jin Y, Wei Z, Gao R, Günaydin H, et al. Deep learning enables cross-modality super-resolution in fluorescence microscopy. *Nat Methods.* 2019; 16: 103-10.
106. van Sloun RJG, Solomon O, Bruce M, Khaing ZZ, Eldar YC, Mischi M. Deep Learning for Super-Resolution Vascular Ultrasound Imaging. *Int Conf Acoust Spee.* 2019: 1055-9.
107. Qiu DF, Zhang SX, Liu Y, Zhu JQ, Zheng LX. Super-resolution reconstruction of knee magnetic resonance imaging based on deep learning. *Comput Meth Prog Bio.* 2020; 187.
108. Harma AS, Ramanik MP. Convolutional neural network for resolution enhancement and noise reduction in acoustic resolution photoacoustic microscopy. *Biomed Opt Express.* 2020; 11: 6826-39.
109. Yao J, Xia J, Maslov KI, Nasirivanaki M, Tsytarev V, Demchenko AV, et al. Noninvasive photoacoustic computed tomography of mouse brain metabolism *in vivo*. *Neuroimage.* 2013; 64: 257-66.
110. Li Y, Gong X, Liu C, Lin R, Hau W, Bai X, et al. High-speed intravascular spectroscopic photoacoustic imaging at 1000 A-lines per second with a 0.9-mm diameter catheter. *J Biomed Opt.* 2015; 20: 065006.
111. Lin R, Li Y, Chen J, Song L. Full field-of-view photoacoustic endoscopy *in vivo*. *SPIE;* 2017.
112. Wu P, Liu K, Zhang Q, Xue ZW, Li YB, Ning NA, et al. Detection of mouse liver cancer via a parallel iterative shrinkage method in hybrid optical/microcomputed tomography imaging. *J Biomed Opt.* 2012; 17.
113. Weber J, Beard PC, Bohndiek SE. Contrast agents for molecular photoacoustic imaging. *Nat Methods.* 2016; 13: 639-50.